Determining Limits of Detection for Different Detector Geometries through Monte Carlo based Simulations

Samuel J. Fearn[1], Samuel R. White[2], Dean T. Connor[3], Euan L. Connolly[1], and Peter G. Martin[1]

[1]Interface Analysis Centre, School of Physics, H.H. Wills Physics Laboratory, Tyndall Avenue, University of Bristol BS8 1TL, UK
[2]Jacobs, 601 Faraday Street, Birchwood Park, Warrington, WA3 6GN, UK
[3]National Nuclear Laboratory, 5th Floor, Chadwick House, Birchwood Park, Warrington, WA3 6AE

Abstract

The threat from nuclear terrorism represents a complex challenge for global governments. Although current systems for detecting threats from illicit materials exist, each have inherent limitations. However, it is crucial that a system can detect when material is being transported with malicious intent and where the potential damage caused by the distribution of such material is likely to require extensive cleanup operations. One monitoring approach comprises the use of a network(s) of distributed detectors in an attempt to detect anomalous events. Quantifying the limits of detection for these small-volume and portable systems is a challenging, but vital, task. Existing work in designing a threat reduction system has not shown a good understanding of what the system is capable of detecting. To rectify this issue, work has been undertaken to create a numerical simulation capable of modelling a moving detector and stationary source with a given distance of closest approach. The algorithm is then able to estimate limits on parameters where the source stops being detectable, by cycling through variables and completing numerous pseudo-experiments at each value. Such an approach will allow any proposed network to ascribe an estimate of the threats that it will be sensitive to. Supplementary work was completed to empirically verify the simulated results. These real-world tests provided confidence that the simulations approximate the physics modelled.

1 Introduction

The monitoring of nuclear material is essential for the purposes of national security. Proliferation of nuclear or radioactive material could allow for the creation of improvised nuclear explosive devices (INEDs), or radiological dispersal devices (RDDs). Such devices are simple; comprising of an explosive device with radioactive material which is dispersed upon detonation. If attempts were made to detonate such a device in an area with high population density, there would be extensive evacuation and cleanup operations required. In the interests of mitigating these attempts, screening for nuclear material is completed at borders, ports and at key strategic targets.

Recent events have shown the possibility for radioactive material to be lost [1]. Though this was not proliferated, it shows the potential for material to fall outside of regulatory control. Most high-activity gamma-ray, γ, sources are currently used for industrial purposes (which have high potential for proliferation) [2]. Due to their larger ranges in air, γ and neutron, n, radiation are the only forms of radiation detectable at appreciable stand-off distances [3], hence, it is γ & n that is screened for by existing detectors. In certain detector systems, through gamma spectroscopy, specific isotopes can be identified by determining the photon energies being emitted.

1.1 Current Screening Methods

The main threat detection and screening system deployed in the UK is "Programme CYCLAMEN" managed by the Atomic Weapons Establishment (AWE) [4]. This system requires people, traffic and cargo at borders to

travel through large polyvinyl-toluene (PVT) scintillating radiation portal monitors (RPMs). Portal monitors are ideal for achieving the high throughput required for cargo and traffic.

Many of these RPMs are PVT based detectors, comprising plastic scintillation based detectors which can detect gamma-rays and, due to their composition of low atomic mass elements, also have some neutron detection capabilities [5]. However, as the compton scattering in plastic scintillators is the dominant mechanism for detection, there is a large range of energies deposited in the detector [6]. This results in insufficient energy resolution which cannot be used for accurate spectral identification of isotopes. The benefits of plastic scintillators are that they are cheap to produce in large volumes and so are a good choice for RPMs which have large cross-sections and require a large amount of scintillating material [7].

Large volume detectors increase the sensitivity to threats. However, screening involving PVT RPMs requires multiple screening stages because they cannot identify material present [8]. The necessity of a second stage in order to determine what material is present and the level of the threat means that it is inefficient and costly, as it requires human intervention and slows the flow of traffic (either vehicles or cargo). As a result and due to the risk of these systems missing threats or being avoided altogether, further threat reduction methods which can catch material in transit should be examined. Distributed detection systems capable of screening personnel in real-time without the need for reduced or directed traffic flow are desirable for these qualities. In this work, distributed detection systems are examined, with an aim to improve their design and implementation.

1.2 Proposed Distributed Detection Systems and Associated Data Analysis Approaches

A distributed detector method currently deployed in the UK is AWE's "Project SIGMA", derived from the US Defense Advanced Research Projects Agency (DARPA) programme of the same name [9]. Although specific details about this project are not available, the system is comprised of a number of large volume NaI(Tl) scintillating detector nodes and some smaller, portable detectors distributed in high traffic areas or carried by police. The large amount of data from this network is analysed by AWE for anomalies as it is streamed to the cloud. The goal is to intercept any threatening material found to be in transit. Methods for alarming are currently being investigated, including the use of signal to noise ratios for raw counts and principal component analysis (PCA) based approaches for anomaly detection in spectral data.

Another US DARPA project, the Mobile Urban Radiation Search (MURS) system was created and tested for the real-time identification and localisation of stationary sources [10]. It uses six 2" $\times$4" $\times$16" NaI(Tl) detectors. A Poisson-Clutter Split (PCS) algorithm is applied for detection and identification.This works by comparing an incoming spectrum to a reference set of background spectra. These are split into their principle components, and a model is trained using the components of the background in the region to determine likelihood of the incoming spectrum belonging to the background set [11]. The main problem with MURS is the cost of such large scintillator crystals. This high cost, renders the MURS system impractical for large scale deployment. However, the PCS algorithm provides a robust and intelligent method of source detection.

Many of these detector and analysis systems intend to use networks of detectors with data being analysed by a single computer [12]. This idea has many advantages such as covering wide areas and allowing anomaly detection and localisation in real-time and in urban and complex environments [13]. There is also a need for some quantification of "normal" levels of radiation. A detector network would allow background to be measured over a large area. Such an approach has benefits for nuclear security internationally, as an increase in radiation levels over a region could indicate a nuclear event elsewhere. The methods proposed could utilise many static or moving detectors all analysed by a single system.

However, the key issue remains in that detector placement is non-trivial - with shielding and large stand-off distances contributing to low detection likelihoods. Much of the work so far does not attempt to quantify whether a detector will have enough signal to flag a threat. It is therefore important to be able to estimate the limit of detection (LoD) - the range of parameters observable by a node in a network, before deploying the system. This work aimed to solve that problem by performing calculations of the LoD for a specific detector geometry and radioactive source. The method can also be used for other LoD calculations, with known or required parameters constrained by the user.

When deciding on the hardware requirements for a detector network, simulations in python, and in GEANT4 or MCNP, should be run to determine the LoD for each detector. This can then be used to inform requirements

such as minimum detecting volume; maximum speed of patrol vehicles; and maximum distance between nodes. It is important that more complex simulation frameworks are used to do calculations as the whole radiation transport can be considered by these toolkits [14], [15]. Python will provide a good first estimate for parameters in experimental design. The idea is that by determining the LoD for a system for simple alarm criteria (determination of a threat), improvement can be shown when using more intelligent criteria, which will also be investigated in future work.

2 Simulation

2.1 Methods

The simulations run here were Monte Carlo (MC) based, meaning that they utilise random variables to model radioactive decay and therefore counts recorded. By defining source position, detector position and detector geometry, counts at each discrete time step can be calculated in the cases where a detector or source is moving. In this way, it is possible to model a detector being driven past a static source, or other dynamic threat scenarios.

Background counts were generated randomly from a Poisson distribution using a user defined mean background count. These were derived empirically by measuring the background of the area with the detector modelled. Alternatively, if simulations are being run for a specific geometry prior to obtaining the detector, the background can be estimated using a simulated environment (based on the environment of the deployment) in GEANT4. The counts from the source were calculated using the source activity, isotope and detector efficiencies, including some shielding. Here, sources were assumed to be spherical point sources, which is reasonable providing the sources are small and relatively far away from the detector.

In a separate MC simulation, many paths were generated from the source, and their trajectory checked for intersections with the detector. The fraction of generated paths that passed through the detector were then used to determine the geometric efficiency, ϵ_{geo}, of the detector/source geometry. The geometric efficiency is given by:

$$\epsilon_{geo} = \frac{\Omega}{4\pi}, \tag{2.1}$$

where Ω is the solid angle subtended by the detector [3]. In cases with complex geometries and where the source/detector geometry is dynamic, it is easier to estimate these ϵ_{geo} values through simulation than calculating them directly [16][17]. This is done by dividing the number of paths which intersect with the detector volume by the total number of paths generated once a sufficiently large number of intersections have been recorded. For this work, 1000 hits were required in the detector volume for a calculation of geometric efficiency for each distinct set of detector coordinates. An example of one possible geometry with paths of gamma-rays from the source is shown in Figure 1.

The mean path length, $\bar{\lambda}_X$, through the detector was used to estimate the intrinsic efficiency, ϵ_{int}, for each geometry with detector material X. When combined with the likelihood of photon interaction in the detector material, it is possible to calculate a value for ϵ_{int}. This is given by:

$$\epsilon_{int} = 1 - e^{-\mu_X \bar{\lambda}_X}, \tag{2.2}$$

where μ_X is the photon attenuation coefficient of material X [3]. These attenuation coefficients account for any possible scattering or absorption of the photon travelling through a given material. It is important to note that attenuation coefficients are a function of photon energy. Therefore, for isotopes with more than one gamma decay energy, different values are needed to account for attenuation [18].

A library of ϵ_{geo} and ϵ_{int} was collated, so that different relative detector/source positions had distinct efficiency values. The python simulation then looked up the available geometry which was the closest match to the simulated setup and used the efficiencies reported.

Attenuation due to obstacles between the source and detector was also accounted for. This was calculated using:

$$T = e^{-(\mu_a \bar{\lambda}_a + \mu_b \bar{\lambda}_b + \ldots)} \tag{2.3}$$

where a, b, etc. are the materials of obstacles in the path of the photon [19].

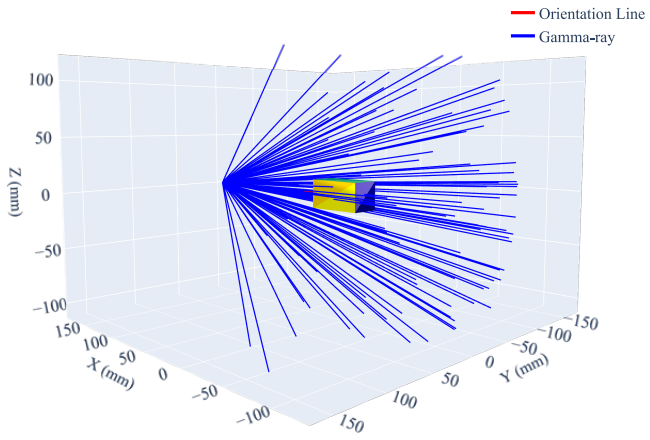

Figure 1: MC simulation of photon paths from a 0.5mm spherical source which intersect with detector volume. From the fraction of total generated paths that intersect with the detector, the geometric efficiency is estimated. In this example, the $50.8 \times 25.4 \times 25.4$ mm^3 detector is 150mm away from the source centre and a geometric efficiency of $\epsilon_{geo} = 0.0222$ is estimated.

Given information about the source, the total source intensity incident on the detector, I, can be calculated using:

$$I = AYT\epsilon_{geo}\epsilon_{int}, \tag{2.4}$$

where A is source activity and Y is the photon yield per second from that isotope [3]. These values were then sampled using a random Poisson variable to give simulated counts. Background counts were added to this value and here, only gross counts are considered.

In this work, simulations were run to calculate the LoD for a $38 \times 38 \times 25$ mm^3 CsI(Tl) detector. 10,000 pseudo-experiments, each consisting of a single pass of the detector past the source, were run for each limit determination. Each pseudo-experiment consists of a distinct sampling of the Poisson distributed intensities which have been calculated. The fraction of these which result in a detection was calculated for a 95% confidence level and the corresponding limiting parameter was reported. The detection criterion was that counts reported by the detector at any given step along the path should be greater than $\mu+3\sigma$, where μ and σ are the mean and standard deviation of the Poisson distributed background counts. If a pseudo-experiment met this requirement then it was recorded as a success.

Pseudo-experiments were run for a range of distances of closest approach between the source and detector, a range of detector speeds and a range of source activities. For each of these parameters, all other values were kept constant. When not the independent variable, the distance of closest approach was fixed at 0.5 m, the velocity at 2 m s^{-1} and the source activity at 360 kBq. These were chosen to allow similarity to the parameters used when testing empirically (see below). In addition, these are reasonable standoff distances and speeds for a vehicle travelling through an RPM - the American National Standards Institute (ANSI) standard being 2.2 m s^{-1} or 1.2 m s^{-1} for a single-sided monitor [20]. The ranges of parameters used for these pseudo-experiments (each with 100 increments) were: 0.1 m to 2 m; 0.5 m s^{-1} to 10 m s^{-1}; and 10 kBq to 5 MBq.

2.2 Results

An example of one pseudo-experiment/simulated run can be seen in Figure 2. This shows the detected counts as x-position of the detector changes with a speed of 0.5 m s^{-1} past a 360 kBq Cs-137 source with a 20 cm distance of closest approach. These parameters are an example of those used in the verification of this model (see next section). Also shown is a plot of the residuals for a fit following the equation:

$$I = \frac{A}{r^2} + C, \tag{2.5}$$

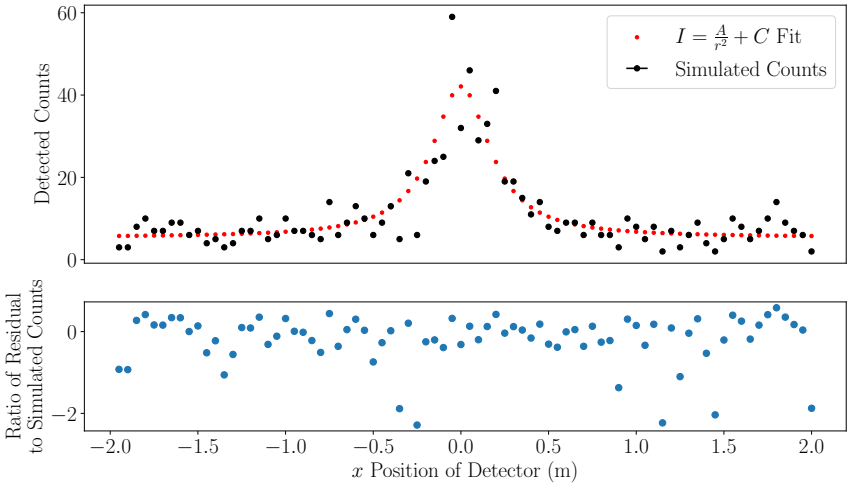

Figure 2: Simulated results for a $38 \times 38 \times 25$ mm CsI(Tl) detector travelling at 0.5 m s^{-1} past a 360 kBq Cs-137 source with a 20 cm distance of closest approach. The simulated counts are fit with a form of the inverse square law for intensity with changing distance. Shielding and attenuation in air has been taken into account in the simulation. The residuals of the fit divided by magnitude of the counts are also plotted and appear to be random, though primarily have negative values. This fit produced a χ^2_ν value of 1.481 and an $\bar{R}^2$ value of 0.772.

where r is the distance between the detector and source, and A and C are unbound constants, determined by the least squares regression fitting method. This equation was chosen for fitting as it is the simplest form of the inverse square law and allows for a baseline background value to be included in the model.

Plots for the fractions of successful pseudo-experiments found over the ranges of parameters listed above can be seen in Figure 3. This shows the expected trends that when increasing activity or decreasing speed or distance to the source, a detection is more probable. At the 95% confidence level, the limiting activity is 620 ± 50 kBq, the limiting speed is 0.8 ± 0.1 m s^{-1}, and the limiting distance is 35 ± 5 cm.

3 Simulation Verification and Validation

To verify and validate this simulation, the procedure described by Naylor and Finger [21] was used to check the similarity between simulated and empirical data using the same parameters. This procedure involves ensuring the model has high face validity. In other words, the model must be a reasonable approximation of the real physical processes. For counts recorded in a detector, the assumption that attenuation coefficients account for all interactions undergone by the source gamma-rays is reasonable. If the energy deposited in the detectors was simulated instead this assumption would fail and the physical processes would need to be modelled individually. When designing a detector network it will be important to model these physical processes more carefully using a particle transport toolkit, as alarm systems may require spectral analysis.

The assumptions of the model were verified by fitting the modelled data with the form of the inverse square law in Equation 2.5. Figures 2, 4 and 5 show simulated results along with their fit and corresponding residuals scaled by the magnitude of the simulated counts for the following parameters respectively: a standoff distance of 20 cm and a detector speed of 0.5 m s^{-1}; a standoff distance of 50 cm and a detector speed of 0.5 m s^{-1}; and a standoff distance of 20 cm and a detector speed of 2 m s^{-1}. For each result, the residuals are approximately random, implying that the model does follow the data well. This also implies that the variance is being accounted for by the model. In addition, all of the reduced chi-squared values, χ^2_ν, are close to 1 (highest and lowest being 1.481 and 0.907 respectively). This means that the data is likely not overfitted and further reassures that the variance of the data is being accounted for by the model.

Reduced coefficients of determination, $\bar{R}^2$, were also calculated for each fit. For the simulations where the

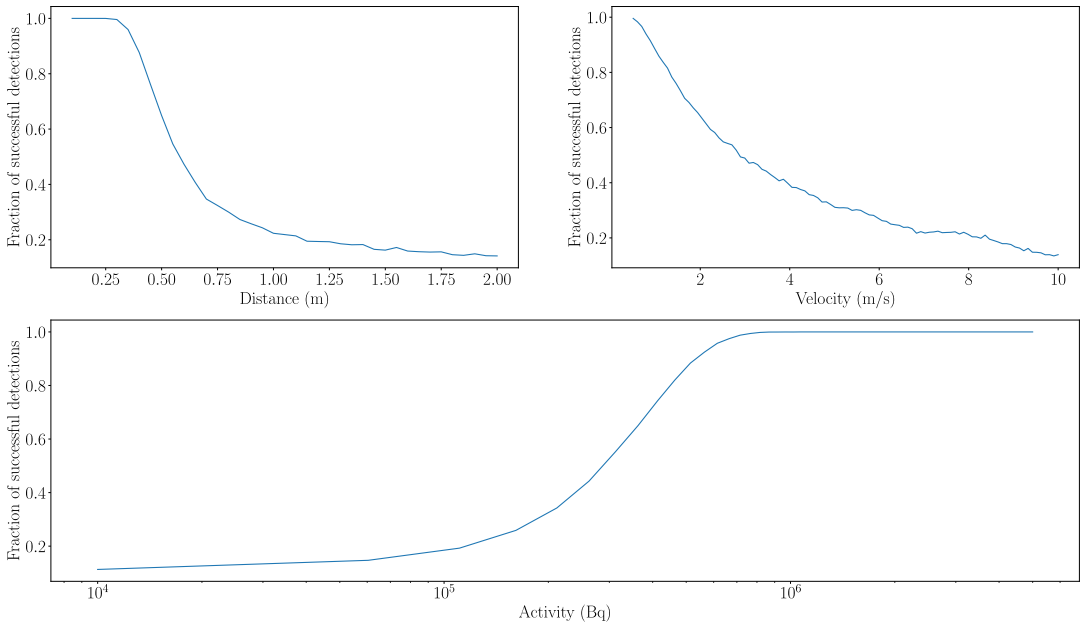

Figure 3: Number of successful pseudo-experiments for increasing distance of closest approach to source (*top left*), detector velocity (*top right*) and source activity (*bottom*). The likelihood of detection increases as distance and velocity decrease and as activity increases. At the 95% confidence level, the limiting activity is 620 ± 50 kBq, the limiting speed is 0.8 ± 0.1 m s^{-1}, and the limiting distance is 35 ± 5 cm.

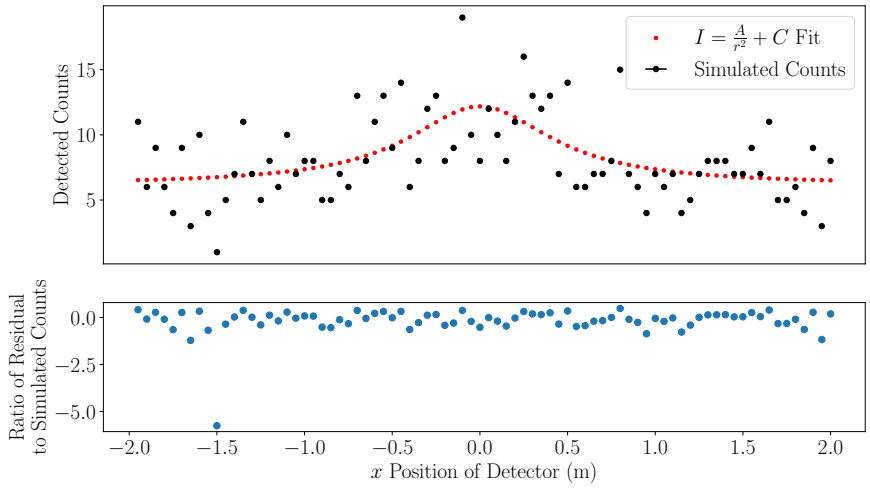

Figure 4: Simulated results for a $38 \times 38 \times 25$ mm CsI(Tl) detector travelling at 0.5 m s^{-1} past a 360 kBq Cs-137 source with a 50 cm distance of closest approach. The simulated counts are fit with a form of the inverse square law for intensity with changing distance. Shielding and attenuation in air has been taken into account in the simulation. The residuals of the fit divided by magnitude of the counts are also plotted and appear to be random, though primarily have negative values. This fit produced a χ^2_ν value of 0.907 and an $\bar{R}^2$ value of 0.277.

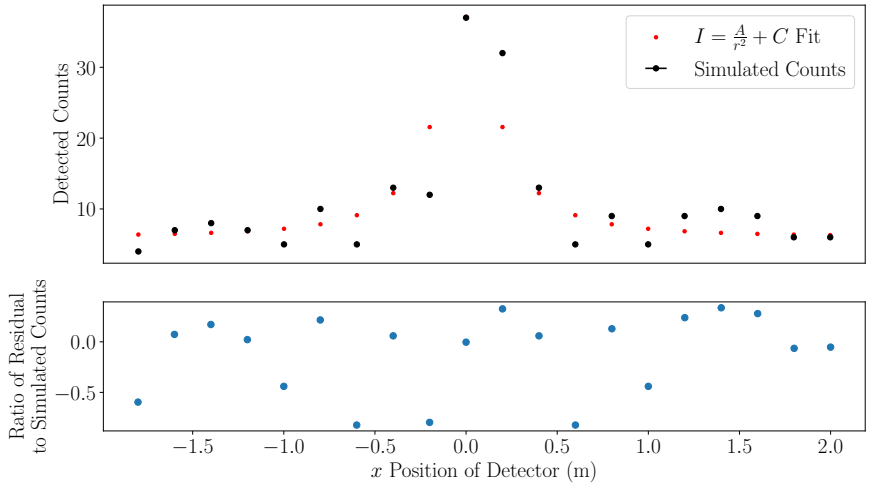

Figure 5: Simulated results for a $38 \times 38 \times 25$ mm CsI(Tl) detector travelling at 2 m s^{-1} past a 360 kBq Cs-137 source with a 20 cm distance of closest approach. The simulated counts are fit with a form of the inverse square law for intensity with changing distance. Shielding and attenuation in air has been taken into account in the simulation. The residuals of the fit divided by magnitude of the counts are also plotted and appear to be random, though primarily have negative values. This fit produced a χ^2_ν value of 1.045 and an $\bar{R}^2$ value of 0.778.

detector was in closer proximity to the source (Figures 2 and 5, for example), the $\bar{R}^2$ values implied a good closeness of fit. However, as can be seen in Figure 4, for lower detector counts, the confidence in the model decreases as the inverse square law becomes less apparent.

Overall, this provides some confidence that the chosen model fits the data well. This means that the simulation behaves as expected, at least for the parameters examined here. It is difficult to say with certainty whether a given model is acceptable for use in a given situation. By keeping the model used here simple, an opportunity for future scrutiny of the simulation using more complicated fits has been afforded.

Finally, the model must be validated by comparing to the results obtained from the real world processes modelled. This has been completed by gathering empirical data as detailed below. This data is compared to the modelled results using hypothesis testing.

3.1 Experimental Design and Methods

To validate the simulation, an experiment was conducted involving a modified version of the system described by White et. al in [22]. This used KUKA KR120 robotic manipulator in combination with a Hamamatsu C12137-01 detector attached to the end effector of the robot. A photograph of the system is shown in Figure 6. The system could then be used to simulate a moving vehicle equipped with a detector system. In this way, the robotic arm with attached detection equipment could be accurately moved at a variety of speeds and distances from a radioactive source. Radiation measurements were collected at a sampling rate of 10 Hz and simultaneously matched with positional outputs from the KUKA at a frequency of 100 Hz.

A series of experiments were conducted using the system, using a 360 kBq Cs-137 sealed source in a 0.5 cm thick lead casing. Data was collected for passes of the detector over the source at distances between 10 ± 1 and 60 ± 1 cm and at 4 different speeds: 0.50 ± 0.05, 1.00 ± 0.05, 1.50 ± 0.05 and 2 ± 0.05 m s^{-1}. The data has been fitted with Equation 2.5 and the residuals plotted as before.

3.2 Results and Comparison

Figure 7 shows an example of 4 passes of the detector past the source for a distance of closest approach of 20 ± 1 cm and a speed of 0.50 ± 0.05 ms^{-1}. Error bars are present on the empirical data due to the exact position of

Figure 6: Image captured during a run of the KUKA robotic arm manipulator with a CsI(Tl) detector attached, moving over a 370 kBq Cs-137 source in a 0.5 cm thick lead casing.

the detector being uncertain because of small fluctuations in the timings of reports from the detector.

The results of this analysis are similar to those for the simulated data. The residuals and χ^2_ν value of 1.146 imply that the data is fit well by the model and that the variance is taken into account and the $\bar{R}^2$ value of 0.847 implies a good closeness of fit. Overall, the results of this analysis for the empirical data provides some reassurance that for various parameters, fitting the same model as to the simulated data gives similar results.

To further verify this model, however, a student's T-test was completed. This serves to test whether the two groups are derived from the same distribution with the same mean. One example comparison can be seen in Figure 8, again for a distance of closest approach of 20 cm and a speed of 0.5 m s^{-1}.

The T-test score calculated for this example was 0.360 with a corresponding p-value of 0.720. If using a 5% confidence level hypothesis test, this implies that there is not enough evidence to suggest that the two datasets are not from a distribution with the same means. This gives more confidence that, since we cannot say the means of the two samples are different, the datasets are similar.

4 Conclusions and Future Work

While it is difficult to attribute with unequivocal certainty that any simulation matches real-world physics, this work yields a reasonable estimate of detected gross counts for the examined parameters. The simple fitted model and the empirical verification are in agreement with the results from the simulation and, as a result, yields confidence in the simulated results.

The goal of this work was to provide an estimate of the LoD for a given setup so that enough counts are detected from the source to be useful in detecting threats. The verification and validation seems to support that this goal has been achieved for the detector volume and source type used. Future work could be done to extend this tool to looking into more detector sizes and geometries as well as other isotopes. It may not be feasible to verify the model in all cases, however, as this requires access to all detector sizes and geometries.

Another potential improvement to this work it to use GEANT4 to give distributions of energies deposited in the detector at each step. This could then be used to inform a more intelligent detection criteria which may be more sensitive to detecting threats in complex environments. Using more complex "toolkits" will be an important step when determining whether a network of detectors is suitable for its intended goal. The work completed here provides a first step to ascertaining the LoD and a way of designing experiments with them

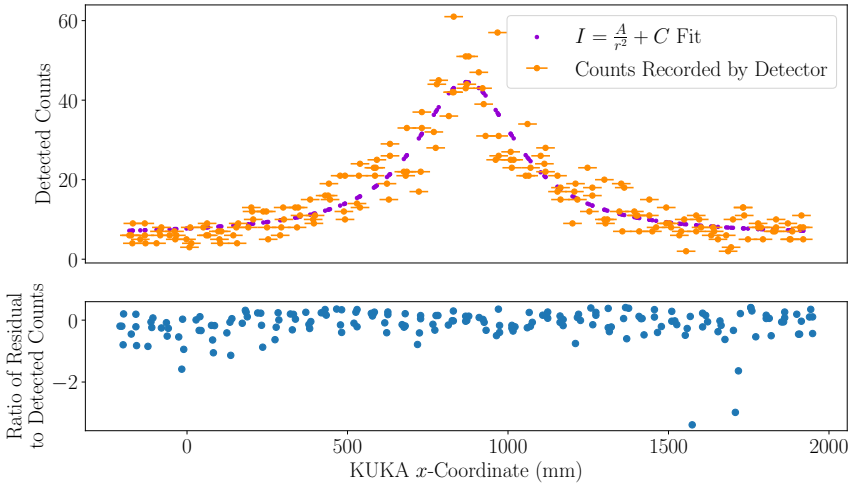

Figure 7: Empirical results for 4 passes of the Hamamatsu C12137-01 detector over a 360 kBq Cs-137 source with a speed of 0.50 ± 0.05 m s^{-1} and a 20 ± 1 cm distance of closest approach. The counts are fit with a form of the inverse square law for intensity with changing distance. The residuals of the fit divided by magnitude of the counts are also plotted and appear to be random, though primarily have negative values. This fit produced a χ^2_ν value of 1.146 and an $\bar{R}^2$ value of 0.847.

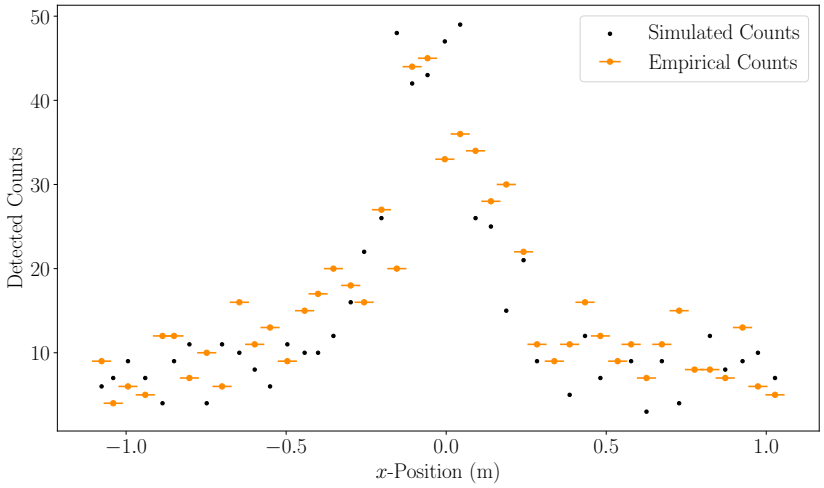

Figure 8: Comparison of simulated and empirical results for a $38 \times 38 \times 25$ mm CsI(Tl) detector travelling at 0.50 ± 0.05 m s^{-1} past a 360 kBq Cs-137 source with a 20 ± 1 cm distance of closest approach. Shielding and attenuation in air has been taken into account in the simulation. These results produced a students T-test score of 0.360 and a p-value of 0.720 suggesting that there is not enough evidence to suggest these datasets are not from the same distribution.

given the resources available.

In addition, this work gives an insight into the "vision" of a handheld detector. This is useful in determining the setup for a network of small scale detectors, if one were to be designed. As expected, the distance of closest approach and relative speed of the source-detector system is important for its detection. For such small detector volumes estimating the limits of detection may be crucial in the setup of a threat screening system.

This work may also serve to assist future emergency response scenarios. If sources are lost, the toolkit outlined in this work could be used to optimize the system deployed for the search. Both aerial and ground mapping and localisation systems can be informed by this simulation. It could also be used to estimate the required approach distances required for ground-based detectors if a nuclear accident occurs, and there is suspected scattered radioactive material.

Overall, this work represents an important method for experimental design and informing the creation of distributed detector networks. There are many other applications for this simulation including the emergency scenarios outlined, source shielding requirements for operator safety, as well as nuclear waste management. While some of the possible parameters have been explored here, this work can also inform other detector characteristics. For example, it could assist in deciding between detector materials and geometries.

References

[1] K. Armstrong, `https://www.bbc.co.uk/news/world-australia-64429375`, Accessed: 12-04-2023, Jan. 2023.

[2] (TECDOC Series 1925). Vienna: International Atomic Energy Agency, 2020.

[3] G. F. Knoll. John Wiley & Sons, Inc., 2010.

[4] R. J. Downes, *Terrorism and Political Violence*, pp. 1–23, Jan. 2019.

[5] J. Ely *et al.*, *Nuclear Instruments and Methods in Physics Research Section A: Accelerators, Spectrometers, Detectors and Associated Equipment*, vol. 560, no. 2, pp. 373–387, 2006.

[6] P. E. Fehlau *et al.*, *IEEE Transactions on Nuclear Science*, vol. 30, no. 1, pp. 158–161, 1983.

[7] E. L. Connolly *et al.*, *Journal of Nuclear Engineering*, vol. 2, no. 3, pp. 246–280, 2021.

[8] R. T. Klann *et al.*, *Nuclear Technology*, vol. 168, no. 1, pp. 79–88, Oct. 2009.

[9] DARPA, `https://www.darpa.mil/news-events/2020-09-04`, Accessed: 25-05-2022, 2020.

[10] J. Curtis *et al.*, *Nuclear Instruments and Methods in Physics Research Section A: Accelerators, Spectrometers, Detectors and Associated Equipment*, vol. 954, Sep. 2018.

[11] B. R. Cosofret *et al.*, in *Chemical, Biological, Radiological, Nuclear, and Explosives (CBRNE) Sensing XV*, A. W. F. III, Ed., International Society for Optics and Photonics, vol. 9073, SPIE, 2014, pp. 253–265.

[12] R. R. Flanagan *et al.*, *Sensors*, vol. 21, no. 6, 2021.

[13] S. Brennan *et al.*, *Computer*, vol. 37, no. 8, pp. 57–59, 2004.

[14] S. Agostinelli *et al.*, *Nuclear Instruments and Methods in Physics Research, Section A: Accelerators, Spectrometers, Detectors and Associated Equipment*, vol. 506, pp. 250–303, 2003.

[15] Los Alamos Scientific Laboratory. Group X-6. Los Alamos, N.M. : Dept. of Energy, Los Alamos Scientific Laboratory ; [Springfield, Va.] : [for sale by the National Technical Information Service], 1979., 1979.

[16] F. Padilla Cabal *et al.*, *Applied Radiation and Isotopes*, vol. 68, no. 12, pp. 2403–2408, 2010.

[17] S. Savović *et al.*, *Measurement Science and Technology*, vol. 21, no. 8, p. 087 002, Jun. 2010.

[18] J. Hubbell, *National Bureau of Standards Report NSRDS-NBS29, Washington DC*, 1969.

[19] W. R. Hendee *et al.* John Wiley & Sons, 2003.

[20] ANSI, *ANSI N42.38-2015 (Revision of ANSI N42.38-2006)*, pp. 1–59, 2016.

[21] T. H. Naylor *et al.*, *Management Science*, vol. 14, no. 2, B92–B101, 1967.

[22] S. R. White *et al.*, *Frontiers in Robotics and AI*, vol. 7, 2020.